A Frictionless Bristle-Based Friction Model That Exhibits Hysteresis and Stick-Slip Behavior☆

Bojana Drinčić[a,*], Dennis S. Bernstein[a]

[a]*Department of Aerospace Engineering, The University of Michigan, Ann Arbor, MI 48109-2140, (734) 764-3719, (734) 763-0578 (FAX)*

Abstract

We investigate the origins of stick-slip friction by developing an asperity-based friction model based on the frictionless and lossless contact between a body and a row of rigid, rotating bristles attached to the ground by torsional springs and dashpots. This model exhibits hysteresis and quasi-stick-slip friction. The hysteretic energy-dissipation mechanism is the sudden release of the compressed bristles, after which the bristles oscillate and the stored energy is dissipated by the dashpot. The discontinuous rotating bristle model is an approximation of the rotating bristle model that exhibits exact stick-slip and hysteresis. We derive a single-state formulation of the discontinuous rotating bristle model and investigate similarities to the LuGre model.

Keywords: friction, hysteresis, stick-slip, LuGre model

1. Introduction

Modeling and control of systems with friction remains a challenging and practically important problem in science and engineering [1–6]. Excessive friction contributes to wasted energy measured in billions of dollars, whereas insufficient friction contributes to accidents. In manufacturing applications, friction is crucial to grinding and polishing, and it is a limiting factor in

achieving precision motion control. In scientific applications, such as atomic force microscopes and nano-scale devices, friction plays a crucial role [7]. A better understanding of friction is essential for improved design, analysis, and prediction.

Experimental observations provide the primary approach to understanding how friction depends on material properties and the relative motion between contacting surfaces [8–10]. Based on these studies, various empirical models have been developed to capture the macroscopic properties of friction [2, 11–19]. These models can be fit to data for a specific application, or they can be used for adaptive control, where parameters are identified and controller gains are updated during operation [13, 20–22]. As discussed in [23], empirical friction models are typically based on an internal state variable, denoted by z, that reflects the internal friction mechanism.

The approach we take to modeling friction is motivated by bristle models [24–26], where the bristles represent the asperities, which determine the macroscopic roughness of the contact surfaces. As the contacting surfaces slide over each other, their asperities touch and are deformed due to shear stresses. Energy is dissipated as the asperities deform and change the shape of the contacting surfaces [2].

The unconventional aspect of the bristle model in the present paper is that the interface between the bristles and the contacting body is frictionless and lossless. The goal of this work is thus to discover how friction and the related phenomenon of hysteresis can emerge from friction-free characteristics. To do this, we construct a hysteretic dissipation mechanism without introducing friction per se. In particular, we assume that each rigid bristle is connected to a spring and a dashpot. As the moving body comes into contact with each bristle, the bristle is deflected and reaction forces occur, but otherwise the contact is lossless and thus frictionless. As the moving body passes beyond a bristle, the bristle is suddenly released, and the potential energy stored in the spring is dissipated by a dashpot regardless of how slowly the body moves. The resulting model is thus hysteretic in the sense that energy dissipation occurs under asymptotically slow motion [27].

In the present paper we analyze the stick-slip behavior of the bristle-based model. We differentiate between *exact stick-slip* and *quasi-stick-slip*. Exact stick-slip refers to motion in which a body attached to a compliance periodically comes to rest. This kind of motion, which is reminiscent of a limit cycle, occurs when the friction force drops as velocity increases from zero; the LuGre model can reproduce stick-slip friction, as can other friction models

[14, 28–34]. Quasi-stick-slip refers to a limit cycle in which forward movement (that is, slip) is followed by a slight backward movement called quasi-slip. Furthermore, we use the steady-state characteristics of the emergent friction force to derive single-state friction models [35] that exhibit stick-slip friction. In particular, we derive the LuGre model [14–17] by this approach.

The contents of the paper are as follows. In Section 2 we introduce the rotating bristle model, derive the governing equations, and show that this model exhibits quasi-stick-slip. In Section 3 we introduce the discontinuous rotating bristle model and show that this model exhibits exact stick-slip and hysteresis. In Section 4 we derive simplified versions of the discontinuous rotating bristle model, including the LuGre model. A preliminary version of some results from this paper is given in [36].

2. Rotating Bristle Model

In this section we describe and analyze the rotating bristle model and demonstrate the emergence of quasi-stick-slip motion. The bristles represent the microscopic roughness of the surface on which the body is sliding as shown in Figure 1. The body of mass m and length d moves over an infinite row of rigid bristles, each of which has length l_b. The position of the center of mass of the body is denoted by x. At the base of each bristle is a torsional spring with stiffness coefficient κ and a torsional dashpot with damping coefficient c. The damping coefficient provides viscous energy dissipation but is otherwise negligible. The mass of each bristle is nonzero but negligible compared to the mass of the body. Therefore, the interaction between each bristle and the body is dominated by the stiffness of the torsional spring. The distance between the bases of adjacent bristles is Δ, and the location of the base of the ith bristle is denoted by x_{b_i}. Furthermore, we assume that the body moves only horizontally, maintaining a constant height h above the ground. The body is not allowed to rotate or move vertically. The distance h can be viewed as the average height of the asperities, which determine the macroscopic roughness of the contacting surfaces. The length $d_0 \triangleq \sqrt{l_b^2 - h^2}$, and we assume throughout this paper that $\frac{d_0}{\Delta} > 1$, so that at every instant there is at least one bristle contributing to the friction force.

As the body moves, there is a frictionless reaction force between the bristle and the body at the point of contact. This force is due to the torsional spring at the base of each bristle. We assume that the force on the body due to contact with the bristle is perpendicular to the direction of the bristle.
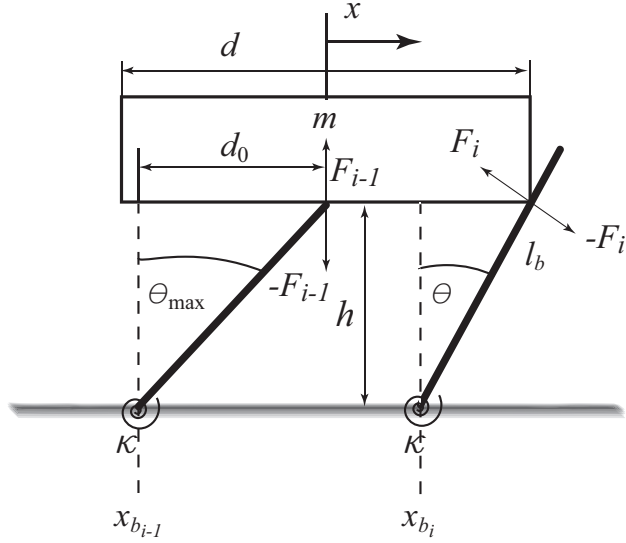
Figure 1: Schematic representation of the body and bristle contact for the rotating bristle model. The body of mass m slides over an infinite row of bristles with negligible mass and length l_b. Each bristle is attached to the ground at its base through a torsional spring with stiffness coefficient κ and a torsional dashpot with damping coefficient c. The distance between the bases of adjacent bristles is Δ, and the location of each bristle is denoted by x_{b_i}. The frictionless reaction force at the point of contact between the body and the ith bristle is F_i.

The sum of all horizontal forces exerted by the bristles at each instant is defined to be the friction force. Since the bristle-body contact is frictionless, the direction of the reaction force between the body and each bristle contacting the lower surface of the body is vertical, and thus these bristles do not contribute to the friction force. Only the bristles that are in contact with the lower corners of the body contribute to the friction force.

For simplicity, we neglect the force due to the dashpot and the bristle dynamics resulting from the impact between the body and the bristle. The torsional dashpot and the bristle mass provide a mechanism for dissipation of the energy stored in the torsional spring but otherwise play no role in the bristle-body interaction. Modeling the impact between the body and each bristle would result in the bristles bouncing off the mass and hitting each other, thus significantly increasing the complexity of the model. Furthermore, we neglect the dynamics of the bristles since they represent the asperities of

the contacting surface, which can deform during the contact, but otherwise exhibit no dynamics.

Furthermore, in simulations of the bristle model throughout this paper we assign numerical values to the bristle-related parameters, such as l_b, Δ, and κ. However, these values do not necessarily represent physically meaningful quantities, but rather serve only to illustrate the interaction between the body and the asperities.

2.1. Bristle pivot angle

The pivot angle of each bristle depends on the position of the bristle relative to the body. Since the body is not allowed to move vertically, the distance h from the ground to the lower surface of the body is constant. The maximum angle $\theta_{\max}$ that a bristle can pivot is given by

$$\theta_{\max} = \cos^{-1}\left(\frac{h}{l_b}\right), \tag{1}$$

and $\theta_{\max} < \frac{\pi}{2}$.

If the ith bristle is pivoted less than $\theta_{\max}$, then its pivot angle θ_i depends on the distance from the position x of the center of the mass of the body to the location x_{b_i} of the base of the ith bristle. If the bristle is in contact with the right lower corner of the body, then $\theta_i = \theta_i^r$, where

$$\theta_i^r = \tan^{-1}\left(\frac{x + \frac{d}{2} - x_{b_i}}{h}\right) \geq 0. \tag{2}$$

If the bristle is in contact with the left lower corner of the body, then $\theta_i = \theta_i^l$, where

$$\theta_i^l = \tan^{-1}\left(\frac{x - \frac{d}{2} - x_{b_i}}{h}\right) \leq 0. \tag{3}$$

We use the pivot angle of each bristle to calculate its contribution to the friction force.

2.2. Friction force

The friction force is equal to the sum of the horizontal components of all of the contact forces between the body and the bristles that are pivoted less

than $\theta_{\max}$ and thus are in contact with one of the lower corners of the body. When the ith bristle is in contact with either the left or right lower corner of the body and pivoted by the angle θ_i, the distance from the base of the ith bristle to the point at which the contact force acts is

$$r_i = \frac{h}{\cos \theta_i},\tag{4}$$

the contact force between the body and the ith bristle is

$$F_i = \frac{\kappa \theta_i}{r_i} = \frac{\kappa \theta_i \cos \theta_i}{h},\tag{5}$$

and the horizontal component of the contact force (5) due to the ith bristle is

$$F_{fi} = F_i \cos \theta_i = \frac{\kappa \theta_i (\cos \theta_i)^2}{h}.\tag{6}$$

To describe the friction force that results from the interaction between the bristles and the body, we define $\Theta_r \in \mathbb{R}^n$ to be the vector whose entries are the pivot angles θ_i^r of the bristles in contact with the right lower corner of the body. Likewise, $\Theta_l \in \mathbb{R}^n$ is the vector whose entries are the pivot angles θ_i^l of the bristles in contact with the left lower corner of the body. We define $\mathcal{X}_b^r(x)$ to be the set of base positions x_{b_i} of the bristles in contact with the right lower corner of the body and $\mathcal{X}_b^l(x)$ to be the set of base positions x_{b_i} of the bristles in contact with the left lower corner of the body. The pivot angles θ_i^r and θ_i^l are calculated by using the elements of the sets $\mathcal{X}_b^r(x)$ and $\mathcal{X}_b^l(x)$ in (2) and (3), respectively. The elements of $\mathcal{X}_b^r(x)$ and $\mathcal{X}_b^l(x)$ are determined based on the position and velocity of the body by using the rules outlined in Table 1, where x_{r-} is the base position of the rightmost bristle contacting the lower surface of the body at the instant the velocity changes sign from negative to positive, and x_{r+} is the base position of the leftmost bristle contacting the lower surface of the body at the instant the velocity changes sign from positive to negative.

Figure 2 illustrates the bristle-body contact scenarios described in Table 1. Figure 2(a) shows the bristle-body interaction starting at the instant the sign of the velocity changes from negative to positive. As the body moves, the bristles that contribute to the friction force change, and so do the sets $\mathcal{X}_b^r(x)$ and $\mathcal{X}_b^l(x)$. In Figure 2(a)-(1) the body starts moving to the right, and all the

Velocity	Position	$\mathcal{X}_b^r(x)$, $\mathcal{X}_b^l(x)$	Description
	$x + \frac{d}{2} \le x_{r-} + \Delta$	$\mathcal{X}_b^l = \{x_{b_i} : x - \frac{d}{2} \le x_{b_i} < x - \frac{d}{2} + d_0\}$ $\mathcal{X}_b^r = \varnothing$	Figure 2(a)-(1)
	$x_{r-} + 2\Delta > x + \frac{d}{2} \ge x_{r-} + \Delta$	$\mathcal{X}_b^l = \{x_{b_i} : x - \frac{d}{2} \le x_{b_i} < x - \frac{d}{2} + d_0\}$ $\mathcal{X}_b^r = \{x_{b_i} : x_{r-} + \Delta \le x_{b_i} < x + \frac{d}{2}\}$	Figure 2(a)-(2)
$v \ge 0$	$x + \frac{d}{2} \ge x_{r-} + 2\Delta$ $x_{r-} - d_0 \ge x - \frac{d}{2}$	$\mathcal{X}_b^l = \{x_{b_i} : x - \frac{d}{2} \le x_{b_i} < x - \frac{d}{2} + d_0\}$ $\mathcal{X}_b^r = \{x_{b_i} : x + \frac{d}{2} - d_0 < x_{b_i} \le x + \frac{d}{2}\}$	Figure 2(a)-(3)
	$x_{r-} \ge x - \frac{d}{2} > x_{r-} - d_0$	$\mathcal{X}_b^l = \{x_{b_i} : x - \frac{d}{2} \le x_{b_i} \le x_{r-}\}$ $\mathcal{X}_b^r = \{x_{b_i} : x + \frac{d}{2} - d_0 < x_{b_i} \le x + \frac{d}{2}\}$	Figure 2(a)-(4)
	$x - \frac{d}{2} > x_{r-}$	$\mathcal{X}_b^l = \varnothing$ $\mathcal{X}_b^r = \{x_{b_i} : x + \frac{d}{2} - d_0 < x_{b_i} \le x + \frac{d}{2}\}$	Figure 2(a)-(5)
	$x - \frac{d}{2} > x_{r+} - \Delta$	$\mathcal{X}_b^l = \varnothing$ $\mathcal{X}_b^r = \{x_{b_i} : x + \frac{d}{2} - d_0 < x_{b_i} \le x + \frac{d}{2}\}$	Figure 2(b)-(1)
	$x_{r+} - 2\Delta < x - \frac{d}{2} \le x_{r+} - \Delta$	$\mathcal{X}_b^l = \{x_{b_i} : x - \frac{d}{2} < x_{b_i} \le x_{r+} - \Delta\}$ $\mathcal{X}_b^r = \{x_{b_i} : x + \frac{d}{2} - d_0 \le x_{b_i} \le x + \frac{d}{2}\}$	Figure 2(b)-(2)
$v < 0$	$x - \frac{d}{2} \le x_{r+} - 2\Delta$ $x_{r+} + d_0 \le x + \frac{d}{2}$	$\mathcal{X}_b^l = \{x_{b_i} : x - \frac{d}{2} \le x_{b_i} < x - \frac{d}{2} + d_0\}$ $\mathcal{X}_b^r = \{x_{b_i} : x + \frac{d}{2} - d_0 < x_{b_i} \le x + \frac{d}{2}\}$	Figure 2(b)-(3)
	$x_{r+} \le x + \frac{d}{2} < x_{r+} + d_0$	$\mathcal{X}_b^l = \{x_{b_i} : x - \frac{d}{2} < x_{b_i} \le x - \frac{d}{2} + d_0\}$ $\mathcal{X}_b^r = \{x_{b_i} : x_{r+} \le x_{b_i} \le x + \frac{d}{2}\}$	Figure 2(b)-(4)
	$x + \frac{d}{2} < x_{r+}$	$\mathcal{X}_b^l = \{x_{b_i} : x - \frac{d}{2} \le x_{b_i} < x - \frac{d}{2} + d_0\}$ $\mathcal{X}_b^r = \varnothing$	Figure 2(b)-(5)

Table 1: The sets $\mathcal{X}_b^r(x)$ and $\mathcal{X}_b^l(x)$ as a function of the position and velocity.

bristles in contact with the body are pivoted counterclockwise, that is, $\theta_i < 0$. The resulting friction force causes the body to accelerate to the right while $x + \frac{d}{2} < x_{r-} + \Delta$. The body encounters the first bristle to its right in Figure 2(a)-(2). As the body continues to move to the right, its right lower corner comes in contact with additional bristles since $x + \frac{d}{2} \ge x_{r-} + 2\Delta$, and bristles push on both lower corners of the body as shown in Figure 2(a)-(3). In Figure 2(a)-(4) the left lower corner of the body is in contact with the only remaining bristle with $\theta_i < 0$, located at x_{r-}. Finally, as the left lower corner of the body passes the base of the bristle located at x_{r-}, that is, $x - \frac{d}{2} > x_{r-}$, only bristles with $\theta_i > 0$ remain in contact with the body as shown in Figure 2(a)-(5). Figure 2(b) shows the bristle-body interaction starting at the instant the sign of the velocity changes from positive to negative. The direction reversal described in Figure 2(b) is analogous to Figure 2(a).

All simulations start at $t = t_0$ with the body position $x = x_0$, and the sets $\mathcal{X}_b^l$ and $\mathcal{X}_b^r$ are assumed to be empty at $t = t_0$. That is, at the begin-
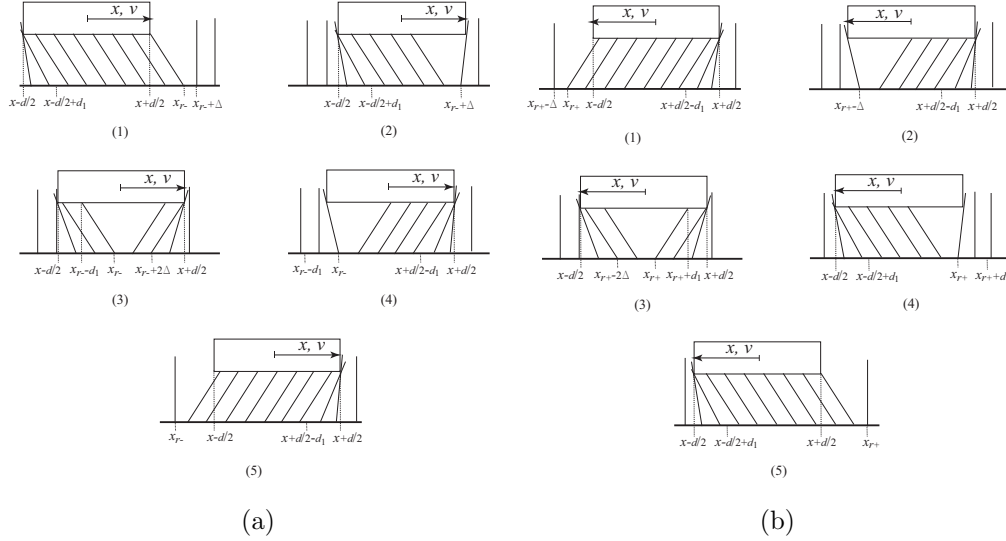
Figure 2: Interaction of the body and bristles during reversals of the body's motion. (a) shows the bristle-body interaction as the sign of the velocity of the body changes from negative to positive. Bristle-body interaction as the sign of velocity of the body changes from positive to negative is shown in (b).

ning of all simulations, the only bristles contacting the body are the bristles contacting the bottom surface of the body and supporting the weight of the body. Therefore, no bristles are in contact with the right or left lower corners of the body at $t = t_0$. The friction force is thus zero and the body encounters bristles according to the rules outlined in Table 2.

Once the sets $\mathcal{X}_b^r(x)$ and $\mathcal{X}_b^l(x)$ are known, the horizontal component of the contact force due to all of the bristles in contact with the right lower corner of the body is

$$F_f^r = \frac{\kappa}{h}\Theta_r^{\mathrm{T}}\left(\cos\Theta_r \circ \cos\Theta_r\right), \tag{7}$$

where "∘" denotes component-wise vector multiplication and the function $\cos(\cdot)$ operates on each component of its vector argument. Likewise, the horizontal component of the contact force due to all of the bristles in contact

8

Velocity	Position	$\mathcal{X}_b^r(x),\ \mathcal{X}_b^l(x)$
$v \geq 0$	$x < x_0 + d_0$	$\mathcal{X}_b^l = \varnothing$ $\mathcal{X}_b^r = \{x_{b_i} : x_0 + \frac{d}{2} < x_{b_i} \leq x + \frac{d}{2}\}$
	$x \geq x_0 + d_0$	$\mathcal{X}_b^l = \varnothing$ $\mathcal{X}_b^r = \{x_{b_i} : x + \frac{d}{2} - d_0 < x_{b_i} \leq x + \frac{d}{2}\}$
$v < 0$	$x > x_0 - d_0$	$\mathcal{X}_b^l = \{x_{b_i} : x - \frac{d}{2} \geq x_{b_i} < x_0 - \frac{d}{2}\}$ $\mathcal{X}_b^r = \varnothing$
	$x \leq x_0 - d_0$	$\mathcal{X}_b^l = \{x_{b_i} : x - \frac{d}{2} \geq x_{b_i} < x - \frac{d}{2} + d_0\}$ $\mathcal{X}_b^r = \varnothing$

Table 2: Initialization of sets $\mathcal{X}_b^r$ and $\mathcal{X}_b^l$.

with the left lower corner of the body is

$$F_f^l = \frac{\kappa}{h}\Theta_l^{\mathrm{T}}\left(\cos\Theta_l \circ \cos\Theta_l\right). \tag{8}$$

The total friction force is thus

$$F_f = F_f^l + F_f^r, \tag{9}$$

where $\mathcal{X}_b^r(x)$ and $\mathcal{X}_b^l(x)$ are determined from tables 1 and 2.

For illustration, consider the body moving with the prescribed position $x(t) = A\sin(\omega t)$ and velocity $v(t) = A\omega\cos(\omega t)$, where $A = 5$ m and $\omega = 0.1$ rad/s. The remaining model parameters are $m = 1$ kg, $d = 1$ m, $\kappa = 0.1$ N-m/rad, $\Delta = 0.002$ m, $l_b = 0.1$ m, $h = 0.098$ m, $d_0 = 0.0199$ m. The resulting friction force as a function of position is shown in Figure 3(a) and as a function of velocity in Figure 3(b). The friction force is initially zero and increases as the mass moves and encounters bristles. The friction force drops slightly when a bristle reaches its maximum pivot angle $\theta_{\max}$ and increases when a new bristle comes in contact with the right lower corner of the body. The magnitude of the friction force oscillates around zero when a direction reversal occurs, since bristles push simultaneously on both the right and left lower corners of the body. In contrast with the Coulomb and LuGre friction models [2, 13, 17], Figure 3(b) shows that, as the velocity crosses zero, the friction force does not change sign.

9
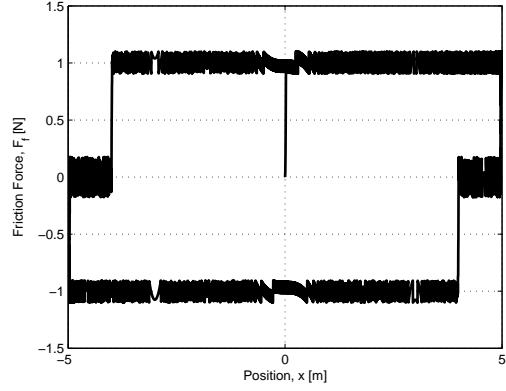
(a)
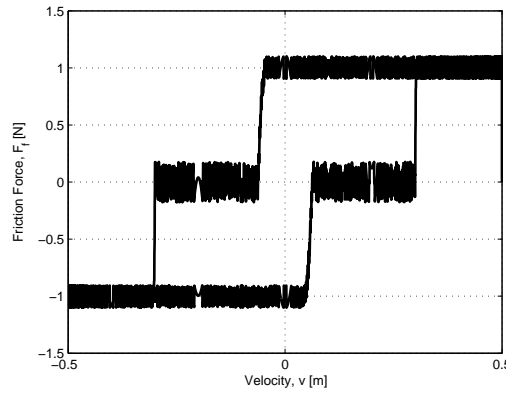
(b)

Figure 3: The friction force (7)-(9) of the rotating bristle model as a function of position (a) and velocity (b). The position of the body is prescribed to be $x(t) = A\sin(\omega t)$ and velocity $v(t) = A\omega\cos(\omega t)$, where $A = 5$ m, $\omega = 0.1$ rad/s.

2.3. Stick-slip behavior

To investigate stick-slip behavior, we simulate the system shown in Figure 4. The body of mass m is connected to a spring with stiffness K. The free end of the spring moves at the constant speed v_p. The equations of motion

are

$$\dot{x} = v, \tag{10}$$

$$\dot{v} = \frac{1}{m}(Kl - F_f), \tag{11}$$

$$\dot{l} = v_p - v, \tag{12}$$

where v is the velocity of the body relative to the ground, l is the length of the spring, and F_f is the friction force described by (7)-(9).
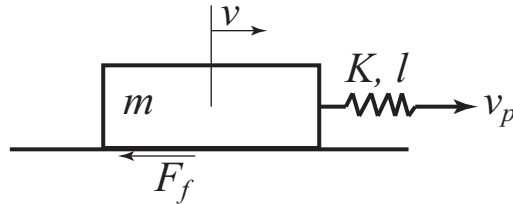

Figure 4: Body-spring configuration used to investigate the stick-slip properties of the rotating bristle model. The body of mass m is connected to a spring with stiffness K. The free end of the spring moves at the constant speed v_p. The friction force F_f is given by (7)-(9).

The results of the simulation of the system (10)-(12) with friction force described by (7)-(9) are shown in Figure 5. The velocity of the free end of the spring is $v_p = 0.5$ m/s, and the model parameters are $\kappa = 0.5$ N-m/rad, $m = 1$ kg, $K = 1$ N/m, $d = 1$ m, $\Delta = 0.01$ m, $d_0 = 0.0199$ m, $l_b = 0.1$ m, and $h = 0.098$ m. The trajectories projected onto the l-v plane form a limit cycle shown in Figure 5(a). The time histories of x, l, v, and F_f are shown in Figure 5(b). As the free end of the spring moves, the spring force overcomes the friction force and the mass accelerates to the right. This is the slip phase. However, as the mass accelerates, the spring length decreases and the friction force becomes larger than the spring force. The body decelerates, momentarily comes to rest, and reverses its direction of motion due to the bristles pushing on it from the right (see Figure 2(b)-(1)). This phase is called *quasi-stick* since, unlike exact stick, the body does not remain stationary. The body moves to the left, its left lower corner comes in contact with bristles, and it continues moving to the left until the friction force becomes negative, corresponding to Figure 2(b)-(5). At this instant, the friction force and the spring force are pushing the body in the same

11

direction, and the body accelerates to the right.
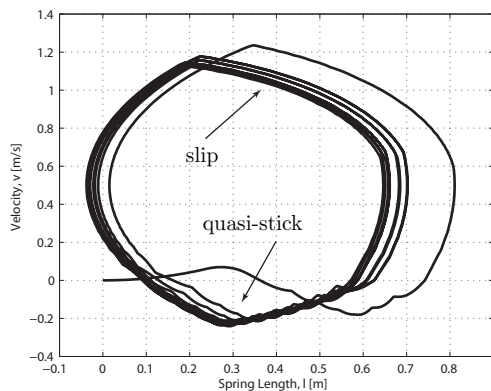
(a)
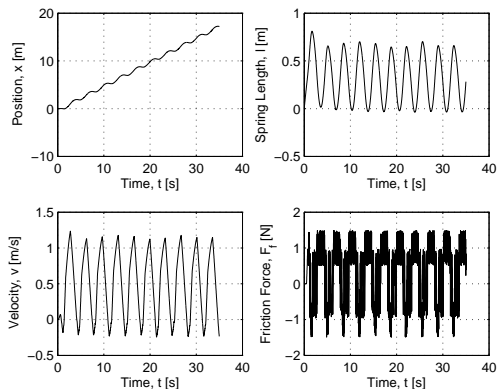
(b)

Figure 5: Quasi-stick-slip limit cycle of the rotating bristle model. The limit cycle in the l-v plane is shown in (a), and the time histories of x, l, v, and F_f are shown in (b).

3. Discontinuous Rotating Bristle Model

In this section, we introduce the discontinuous rotating bristle model (DRBM), which is identical to the rotating bristle model except during direction reversals. In particular, the details of the direction reversals arising in the rotating bristle model are replaced by a simplified model in the DRBM.

12

To construct the DRBM, we assume that when the velocity of the body passes through zero and changes sign from positive to negative, the configuration in which all of the bristles contacting the body are pivoted to the right, $\theta_i \geq 0$, jumps discontinuously to a configuration in which all of the bristles contacting it are pivoted to the left, $\theta_i \leq 0$. Similarly, when the velocity of the body passes through zero and changes sign from negative to positive, the configuration in which all of the bristles contacting the body are pivoted to the left, $\theta_i \leq 0$, jumps discontinuously to the configuration in which all of the bristles contacting it are pivoted to the right, $\theta_i \geq 0$. In figures 2(a) and 2(b) this is equivalent to an instantaneous transition from the configuration in Figure 2(a)-(1) and 2(b)-(1) to the configuration in Figure 2(a)-(5) and 2(b)-(5), respectively, without passing through the configurations described in figures 2(a)-(2), -(3), and -(4) and 2(b)-(2),-(3),-(4), respectively.

The DRBM friction force for $v \geq 0$ is given by

$$F_f = F_f^r, \tag{13}$$

where F_f^r is defined by (7) and the components of Θ_r are given by (2) with x_{b_i} in the set

$$\mathcal{X}_b^r(x) = \{x_{b_i} \ : \ x + \frac{d}{2} - d_0 < x_{b_i} \leq x + \frac{d}{2}\}. \tag{14}$$

Note that, for every value of x, the set $\mathcal{X}_b^r(x)$ is nonempty and is initialized from (14) based on the initial position $x(t_0)$. For $v < 0$, the DRBM friction force is given by

$$F_f = F_f^l, \tag{15}$$

where F_f^l is defined by (8) and the components of Θ_l are given by (3) with x_{b_i} in the set

$$\mathcal{X}_b^l(x) = \{x_{b_i} \ : \ x - \frac{d}{2} \leq x_{b_i} < x - \frac{d}{2} + d_0\}, \tag{16}$$

which, for all values of x, is nonempty and is initialized from (16) based on the initial position $x(t_0)$.

Due to the discontinuous jump from a configuration in which all of the pivot angles satisfy $\theta_i \geq 0$ to a configuration in which all of the pivot angles satisfy $\theta_i \leq 0$, and vice versa, we compare the value of F_f as $v \to 0^+$ with

13

the value of F_f as $v \to 0^-$ in order to determine discontinuities of the friction force at zero velocity. The value of θ_i given by (2) with $x_{b_i} \in \mathcal{X}_b^r(x)$ defined by (14) is in the range

$$0 \leq \theta_i < \tan^{-1}\left(\frac{d_0}{h}\right). \tag{17}$$

Thus, it follows from (13) and (7) that $F_f \geq 0$ for all $v \geq 0$. However, since $\frac{d_0}{\Delta} > 1$, $\mathcal{X}_b^r(x)$ has at least one element, namely, the ith bristle with base at x_{b_i} and $\theta_i > 0$. The contribution of the ith bristle to the friction force F_f is thus nonzero and therefore $F_f > 0$ for all $v \geq 0$. On the other hand, the value of θ_i given by (3) with $x_{b_i} \in \mathcal{X}_b^l(x)$ defined by (16) satisfies

$$-\tan^{-1}\left(\frac{d_0}{h}\right) < \theta_i \leq 0. \tag{18}$$

It follows from (15) and (8) that $F_f \leq 0$ for all $v < 0$. However, since $\frac{d_0}{\Delta} > 1$, $\mathcal{X}_b^l(x)$ has at least one element, namely, the ith bristle with base at x_{b_i} and $\theta_i < 0$. The contribution of the ith bristle to the friction force F_f is thus nonzero and therefore $F_f < 0$ for all $v < 0$.

Since $F_f > 0$ for all $v \geq 0$ and $F_f < 0$ for all $v < 0$, we look for the minimum value of (13) and maximum value of (15). The minimum value of F_f for $v \geq 0$ occurs when only the ith bristle is contributing to the friction force and thus $x_{b_i} = x + \frac{d}{2} - d_0 + \Delta$, $x_{b_i} \in \mathcal{X}_b^r(x)$, and $\theta_i = \tan^{-1}\left(\frac{d_0-\Delta}{h}\right) > 0$. At this instant the pivot angle of the $(i-1)$th bristle reaches $\theta_{\max}$ and no longer contributes to the friction force, that is, $x_{b_{i-1}} = x + \frac{d}{2} - d_0$. Thus, the ith bristle is the only bristle contributing to the friction force, and the minimum value of F_f defined by (13) and (7) for $v \geq 0$ is

$$F_{f,\min} = \frac{k}{h}\tan^{-1}\left(\frac{d_0 - \Delta}{h}\right)\cos^2\left(\tan^{-1}\left(\frac{d_0 - \Delta}{h}\right)\right) > 0. \tag{19}$$

Similarly, the maximum value of F_f for $v < 0$ occurs when only the ith bristle contributes to the friction force and thus $x_{b_i} = x - \frac{d}{2} + d_0 - \Delta$, $x_{b_i} \in \mathcal{X}_b^l(x)$, and $\theta_i = -\tan^{-1}\left(\frac{d_0-\Delta}{h}\right) < 0$. At this instant, the pivot angle of the $(i+1)$th bristle reaches $\theta_{\max}$ and no longer contributes to the friction force, that is $x_{b_{i+1}} = x - \frac{d}{2} + d_0$. Thus, the ith bristle is the only bristle contributing to the friction force, and the maximum value of F_f defined by (15) and (8) for

14

$v < 0$ is

$$F_{f,\max} = -\frac{k}{h}\tan^{-1}\left(\frac{d_0 - \Delta}{h}\right)\cos^2\left(\tan^{-1}\left(\frac{d_0 - \Delta}{h}\right)\right) = -F_{f,\min} < 0.$$

(20)

Comparing (19) with (20) shows that, for all $v \geq 0$, $F_f \geq F_{f,\min} > 0$ whereas, for all $v < 0$, $F_f \leq F_{f,\max} < 0$, where $F_{f,\max} = -F_{f,\min}$. Therefore,

$$\lim_{v \to 0^-} F_f < 0 < \lim_{v \to 0^+} F_f,$$

(21)

which implies that the DRBM friction force F_f defined by (13)-(16) is discontinuous at $v = 0$.

As in the previous section, we consider the body moving with the prescribed position $x(t) = A\sin(\omega t)$ and velocity $v(t) = A\omega\cos(\omega t)$, where $A = 1$ m and $\omega = 0.01$ rad/s. The resulting DRBM friction force as a function of position is shown in Figure 6(a) and as a function of velocity in Figure 6(b). In Figure 6(a), a drop in the friction force appears when a bristle reaches the pivot angle $\theta_{\max}$, making the friction force look like a sawtooth function of position. The friction force of the DRBM does not oscillate around zero during direction reversals as in Figure 3(a). However, the direction of the friction force instantaneously switches while the magnitude remains unchanged, resulting in a discontinuity at $v = 0$ as shown in Figure 6(b). The velocity is zero at $t_1 = \frac{\pi}{2\omega}$ and $t_2 = \frac{3\pi}{2\omega}$, and thus, a discontinuity in friction force is also visible in Figure 6(a) at $x(t_1) = 1$ m and $x(t_2) = -1$ m.

3.1. Switch Model

Due to the discontinuity of the DRBM friction force (13)-(16) at $v = 0$, the integration of (10)-(12) with the friction force represented by the DRBM (13)-(16) requires special numerical techniques. In this section we describe the Switch Model [30, 37], which is a technique that smooths out the discontinuous dynamics around the discontinuity $v = 0$. The modified equations can then be integrated using standard numerical integration techniques.

To begin, we rewrite the equations of motion in which the friction force is modeled by the DRBM as a differential inclusion [37]. Assume that the

15
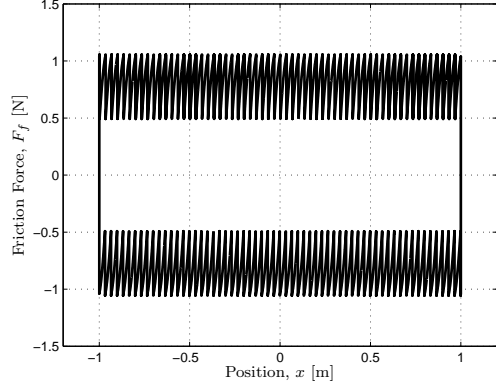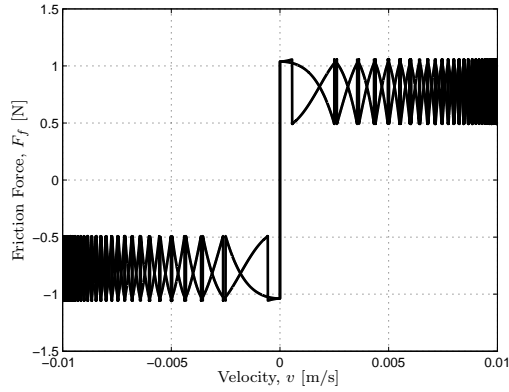
Figure 6: The DRBM friction force (13)-(16) as a function of position (a) and velocity (b). The position of the body is prescribed to be $x = A\sin(\omega t)$, and the velocity $v = A\omega\cos(\omega t)$, where $A = 1$ m, $\omega = 0.01$ rad/s. As shown in (b) the DRBM friction force is discontinuous at $v = 0$.

motion of the body is described by

$$\dot{\boldsymbol{x}} = \boldsymbol{f}(\boldsymbol{x}), \tag{22}$$

where $\boldsymbol{x} \in \mathbb{R}^m$ and $\boldsymbol{f} : \mathcal{V} \subset \mathbb{R}^m \to \mathbb{R}^m$ is a piecewise continuous vector field, and $\Sigma \triangleq \mathbb{R}^m \backslash \mathcal{V}$ is the set of points of discontinuity of $\boldsymbol{f}$. We assume that there exists a function $g : \mathbb{R}^m \to \mathbb{R}$ such that the discontinuity boundary Σ

16

is given by the roots of g, that is

$$\Sigma = \{\boldsymbol{x} \in \mathbb{R}^m : g(\boldsymbol{x}) = 0\}. \tag{23}$$

We also define sets

$$\mathcal{V}_+ \triangleq \{\boldsymbol{x} \in \mathbb{R}^m : g(\boldsymbol{x}) > 0\}, \tag{24}$$

$$\mathcal{V}_- \triangleq \{\boldsymbol{x} \in \mathbb{R}^m : g(\boldsymbol{x}) < 0\}. \tag{25}$$

With these definitions, (22) can be rewritten as the differential inclusion [37, 38]

$$\dot{\boldsymbol{x}} \in \begin{cases} \boldsymbol{f}_+(\boldsymbol{x}), \ \boldsymbol{x} \in \mathcal{V}_+, \\ \alpha\boldsymbol{f}_+(\boldsymbol{x}) + (1-\alpha)\boldsymbol{f}_-(\boldsymbol{x}), \ \boldsymbol{x} \in \Sigma, \ \alpha \in [0,1], \\ \boldsymbol{f}_-(\boldsymbol{x}), \ \boldsymbol{x} \in \mathcal{V}_-. \end{cases} \tag{26}$$

The direction of the flow given by the vector fields $\boldsymbol{f}_+(\boldsymbol{x})$ and $\boldsymbol{f}_-(\boldsymbol{x})$ can lead to three types of sliding modes across Σ. If the flow is such that the solutions of (26) are pushed to Σ in both $\mathcal{V}_+$ and $\mathcal{V}_-$, then the sliding mode is *attractive*. If the solutions cross Σ, then the sliding mode is *transversal*. Finally, if the solutions diverge from Σ, the sliding mode is *repulsive* [37].

The Switch Model smooths out the dynamics of the differential inclusion (26) by constructing a *stick band* within the set $\mathcal{G} \triangleq \{\boldsymbol{x} : |g(\boldsymbol{x})| \leq \eta\}$, where η is a small positive constant. (Note that the term "stick band" is not related to stick-slip friction.) The dynamics outside of the stick band remain the same. The dynamics inside the stick band depend on the type of sliding mode across the discontinuity boundary. If the sliding mode is attractive, that is,

$$\boldsymbol{n}^{\mathrm{T}}\boldsymbol{f}_-(\boldsymbol{x}) > 0 \text{ and } \boldsymbol{n}^{\mathrm{T}}\boldsymbol{f}_+(\boldsymbol{x}) < 0, \quad \boldsymbol{x} \in \Sigma, \tag{27}$$

where $\boldsymbol{n} \triangleq \nabla g(\boldsymbol{x})$ is the normal to Σ, then the stick-band dynamics are given by

$$\dot{\boldsymbol{x}} = \alpha\boldsymbol{f}_+(\boldsymbol{x}) + (1-\alpha)\boldsymbol{f}_-(\boldsymbol{x}), \ \boldsymbol{x} \in \mathcal{G}. \tag{28}$$

The value of the parameter α is chosen such that it pushes the solutions of (27) toward the middle of the stick band, that is, toward $g(\boldsymbol{x}) = 0$. Thus,

17

inside the stick band, g satisfies

$$\dot{g}(\boldsymbol{x}) = -\tau g(\boldsymbol{x}), \tag{29}$$

where $\tau > 0$ is a time constant. Since

$$\dot{g}(\boldsymbol{x}) = \frac{dg(\boldsymbol{x})}{d\boldsymbol{x}} \frac{d\boldsymbol{x}}{dt} = \nabla \boldsymbol{g}^T \dot{\boldsymbol{x}} \tag{30}$$

$$= \boldsymbol{n}^T \left(\alpha \boldsymbol{f}_+(\boldsymbol{x}) + (1 - \alpha) \boldsymbol{f}_-(\boldsymbol{x}) \right), \tag{31}$$

setting (29) equal to (31) and solving for α gives

$$\alpha = \frac{\boldsymbol{n}^T \boldsymbol{f}_-(\boldsymbol{x}) + \tau^{-1} g(\boldsymbol{x})}{\boldsymbol{n}^T (\boldsymbol{f}_-(\boldsymbol{x}) - \boldsymbol{f}_+(\boldsymbol{x}))}. \tag{32}$$

If the sliding mode is transversal, that is,

$$(\boldsymbol{n}^\mathrm{T} \boldsymbol{f}_-(\boldsymbol{x}))(\boldsymbol{n}^\mathrm{T} \boldsymbol{f}_+(\boldsymbol{x})) > 0, \quad \boldsymbol{x} \in \Sigma, \tag{33}$$

then the stick-band dynamics are defined by

$$\dot{\boldsymbol{x}} = \begin{cases} \boldsymbol{f}_-(\boldsymbol{x}), \text{ if } \boldsymbol{n}^\mathrm{T} \boldsymbol{f}_-(\boldsymbol{x}) < 0 \text{ and } \boldsymbol{n}^\mathrm{T} \boldsymbol{f}_+(\boldsymbol{x}) < 0 , \boldsymbol{x} \in \mathcal{G}, \\ \boldsymbol{f}_+(\boldsymbol{x}), \text{ if } \boldsymbol{n}^\mathrm{T} \boldsymbol{f}_-(\boldsymbol{x}) > 0 \text{ and } \boldsymbol{n}^\mathrm{T} \boldsymbol{f}_+(\boldsymbol{x}) > 0 , \boldsymbol{x} \in \mathcal{G}. \end{cases} \tag{34}$$

Finally, if the sliding mode is repulsive, that is,

$$\boldsymbol{n}^\mathrm{T} \boldsymbol{f}_-(\boldsymbol{x}) < 0 \text{ and } \boldsymbol{n}^\mathrm{T} \boldsymbol{f}_+(\boldsymbol{x}) > 0, \quad \boldsymbol{x} \in \Sigma, \tag{35}$$

than the dynamics are defined by

$$\dot{\boldsymbol{x}} = \boldsymbol{f}_+(\boldsymbol{x}), \, \boldsymbol{x} \in \mathcal{G}. \tag{36}$$

Outside of the stick band, the dynamics are defined by

$$\dot{\boldsymbol{x}} = \begin{cases} \boldsymbol{f}_+(\boldsymbol{x}), \, \boldsymbol{x} \in \mathcal{G}_+, \\ \boldsymbol{f}_-(\boldsymbol{x}), \, \boldsymbol{x} \in \mathcal{G}_-, \end{cases} \tag{37}$$

where $\mathcal{G}_+ \triangleq \{\boldsymbol{x} : g(\boldsymbol{x}) > \eta\}$ and $\mathcal{G}_- \triangleq \{\boldsymbol{x} : g(\boldsymbol{x}) < \eta\}$. More details about the Switch Model (27)-(37) and a pseudocode are given in [37].

18

3.2. Stick-slip behavior

We use the Switch Model (27)-(37) to simulate the system shown in Figure 4 and defined by (10)-(12) with friction force defined by the DRBM (13)-(16). The system (10)-(12) with friction force modeled by (13)-(16) can be formulated as a differential inclusion (26) with $\boldsymbol{x} \triangleq \begin{bmatrix} x & v & l \end{bmatrix}^{\mathrm{T}}$, the set Σ defined by the roots of the function $g(\boldsymbol{x}) = v$, the normal to Σ defined by $\boldsymbol{n} = \nabla g(\boldsymbol{x}) = \begin{bmatrix} 0 & 1 & 0 \end{bmatrix}^{\mathrm{T}}$, and the vector fields $\boldsymbol{f}_+(\boldsymbol{x})$ and $\boldsymbol{f}_-(\boldsymbol{x})$ defined by

$$\boldsymbol{f}_+(\boldsymbol{x}) \triangleq \begin{bmatrix} v \\ \frac{1}{m}(Kl - F_{f+}) \\ v_p - v \end{bmatrix}, \tag{38}$$

$$\boldsymbol{f}_-(\boldsymbol{x}) \triangleq \begin{bmatrix} v \\ \frac{1}{m}(Kl - F_{f-}) \\ v_p - v \end{bmatrix}, \tag{39}$$

where $F_{f+} = F_f^r$ is the DRBM friction force for $v \geq 0$ defined by (13) and $F_{f-} = F_f^l$ is the DRBM friction force for $v < 0$ defined by (15).

We use the Switch Model (27)-(37) to simulate the differential inclusion (26) with $\boldsymbol{f}_+(\boldsymbol{x})$ and $\boldsymbol{f}_-(\boldsymbol{x})$ defined by (38) and (39) with $m = 1$ kg, $K = 1$ N/m, $v_p = 0.002$ m/s, $d = 0.5$ N, $\kappa = 0.1$ N-m/rad, $h = 0.0995$ m, $l_b = 0.1$ m, $d_0 = 0.01$ m, $\Delta = 0.005$ m, and $\eta = 10^{-8}$. Part (a) of Figure 7 shows the limit cycle obtained by projecting the trajectories onto the l-v plane, and Figure 7(b) shows the time histories of x, l, v, and F_f. The exact stick-slip motion is represented by the limit cycle in the l-v plane. The quasi-stick phase of the rotating bristle model shown in Figure 5(a) is replaced by sticking, indicated by the line segment in which $v = 0$ and $\dot{l} = v_p$. The exact stick-slip behavior of the DRBM is a consequence of the drop in friction force that occurs when the bristle pivot angle reaches $\theta_{\max}$.

3.3. Hysteresis map

We consider the mass-spring system shown in Figure 8. The body of mass m is attached to the wall by means of a spring with stiffness coefficient K. A periodic force input $u(t)$ acts on the body causing it to move over the horizontal surface. The friction force between the body and the surface is

19
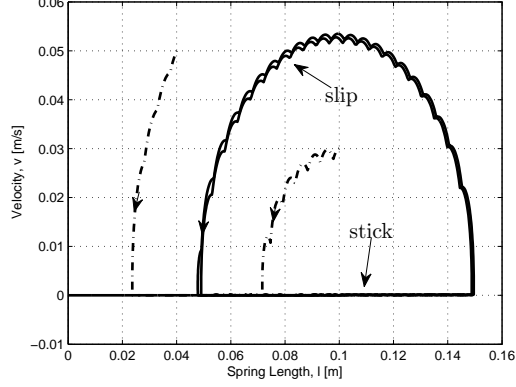
(a)
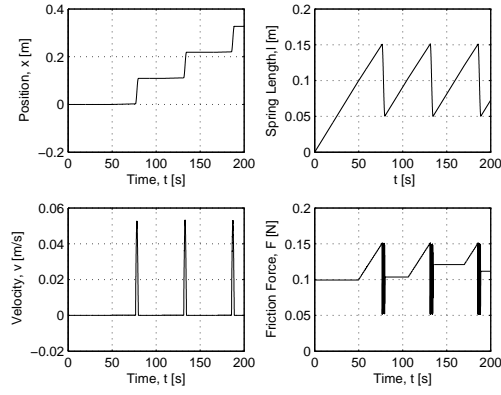
(b)

Figure 7: The exact stick-slip limit cycle of (38)-(39) with friction force modeled by the DRBM (13)-(16). (a) shows the stable limit cycle in the l-v plane. The trajectories starting inside and outside of the limit cycle converge to it. (b) shows the time histories of x, l, v, and F_f with zero initial conditions. The parameter values are $m = 1$ kg, $K = 1$ N/m, $v_p = 0.002$ m/s, $d = 0.5$ N, $\kappa = 0.1$ N-m/rad, $h = 0.0995$ m, $l_b = 0.1$ m, $d_0 = 0.01$ m, $\Delta = 0.005$ m, and $\eta = 10^{-8}$.

represented by the DRBM (13) - (16). The equations of motion are

$$\dot{x} = v, \tag{40}$$

$$\dot{v} = \frac{1}{m}(-Kx + u - F_f). \tag{41}$$

20
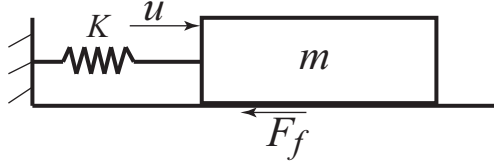
Figure 8: Body-spring configuration represented by (40)-(41). The body of mass m is connected to the wall by a means of a spring with stiffness K and is acted on by an external force input u.

To formulate (40)-(41) with F_f defined by (13)-(16) as a differential inclusion (26), we define vector fields $\boldsymbol{f}_+(\boldsymbol{x})$ and $\boldsymbol{f}_-(\boldsymbol{x})$ corresponding to (40), (41) by

$$\boldsymbol{f}_+(\boldsymbol{x}) \triangleq \begin{bmatrix} v \\ \frac{1}{m}(-Kx + u - F_{f+}) \end{bmatrix}, \tag{42}$$

$$\boldsymbol{f}_-(\boldsymbol{x}) \triangleq \begin{bmatrix} v \\ \frac{1}{m}(-Kx + u - F_{f-}) \end{bmatrix}, \tag{43}$$

where $\boldsymbol{x} = \begin{bmatrix} x & v \end{bmatrix}^{\mathrm{T}}$, $F_{f+} = F_f^r$ is the DRBM friction force for $v \geq 0$ defined by (13), and $F_{f-} = F_f^l$ is the DRBM friction force for $v < 0$ defined by (15). The set Σ is defined by the roots of the function $g(\boldsymbol{x}) = v$, so that $\boldsymbol{n} = \nabla g(\boldsymbol{x}) = \begin{bmatrix} 0 & 1 \end{bmatrix}^{\mathrm{T}}$.

We utilize the Switch Model (27)-(37) to simulate (26) with $\boldsymbol{f}_+(\boldsymbol{x})$ and $\boldsymbol{f}_-(\boldsymbol{x})$ defined by (42), (43), and the force input $u(t) = \sin(\omega t)$. The system parameters used are $m = 1$ kg, $K = 1$ N/m, $l_b = 0.1$ m, $\kappa = 0.1$ N-m/rad, $d = 1$ m, $h = 0.0995$ m, $\Delta = 0.01$ m, and $\eta = 10^{-6}$. The input-output map of (42)-(43) with $\omega = 0.05$ rad/s is shown in Figure 9(a) and with $\omega = 0.001$ rad/s is shown in Figure 9(b). At low input frequencies, the input-output map forms a loop, showing that the system is hysteretic. The input-output map $\mathcal{H}$, called the hysteresis map, is rate-dependent since its shape changes with the frequency of the input [39]. The staircase shape of the hysteresis map, also observed with the LuGre model, indicates exact stick-slip behavior [11]. The time histories of x, v, u, and F_f for $\omega = 0.001$ rad/s are shown in Figure 9(c).

Since the input-output map of (42)-(43) is hysteretic, we can calculate the energy dissipated during one cycle of operation. The area $\mathcal{A}$ of the hysteresis map $\mathcal{H}$ shown in Figure 9(b) is equal to the energy loss during one cycle. To

(a)   (b)   (c)
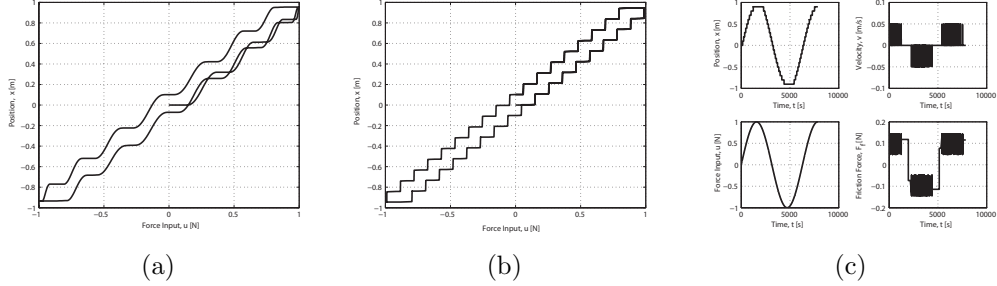
Figure 9: Simulation of (42)-(43) with friction force modeled by the DRBM with $u(t) = \sin(\omega t)$ N, $m = 1$ kg, $K = 1$ N/m, $l_b = 0.1$ m, $\kappa = 0.1$ N-m/rad, $d = 1$ m, $h = 0.0995$ m, $\Delta = 0.01$ m, and $\eta = 10^{-6}$. (a) shows the input-output map with $\omega = 0.05$ rad/s and (b) shows the input-output map with $\omega = 0.001$ rad/s. The shape of the input-output map at low frequencies indicates exact stick-slip behavior. The time histories of x, v, u, and F_f with $\omega = 0.001$ rad/s are shown in (c).

demonstrate, we begin with the expression for work done by the force $u(t)$ during one cycle and use Green's theorem

$$E = \oint_{\mathcal{H}} u dx = \int\int_{\mathcal{A}} du dx = \mathcal{A} \tag{44}$$

to show that the work done E is equal to the area $\mathcal{A}$ of the hysteresis map. The energy dissipated based on the area of the hysteresis loop shown in Figure 9(b) is $E = 0.35647$ J.

Alternatively, we can calculate the dissipated energy by summing the potential energy stored in each torsional spring during the motion of the body. As each bristles pivots, energy is stored in its torsional spring, and is subsequently dissipated by the dashpot after the body passes beyond the bristle and the bristle is suddenly released. The total energy stored in the bristles is

$$E_{\text{stored}} = \frac{1}{2} N_e \kappa \theta_{\text{max}}^2, \tag{45}$$

where N_e is the number of bristles that the mass contacts during one cycle of motion. Based on the minimum x_{min} and maximum x_{max} value of x during

one cycle of motion and the spacing of the bristles, N_e is given by

$$N_e = 2 \left\lfloor \frac{x_{\max} - x_{\min}}{\Delta} \right\rfloor, \qquad (46)$$

where $\lfloor \cdot \rfloor$ denotes integer part. The dissipated energy calculated from (45) is $E_{\text{stored}} = 0.35566$ J.

3.4. Approximation of the friction force

The calculation of the DRBM friction force (13)-(16) requires keeping track of the position of each bristle relative to the body. In order to simplify the calculation of F_f, we note that the friction force of the DRBM is a function of position that resembles a sawtooth wave as shown in Figure 6(a). Thus, the friction force (13)-(16) can be approximated by the sawtooth wave

$$F_f = \begin{cases} F_f^r, \ v \geq 0, \\ F_f^l, \ v < 0, \end{cases} \qquad (47)$$

$$F_f^r \approx F_{\min} + \frac{F_{\max} - F_{\min}}{\Delta} \operatorname{mod}(x, \Delta), \qquad (48)$$

$$F_f^l \approx - \left(F_{\min} + \frac{F_{\max} - F_{\min}}{\Delta} \operatorname{mod}(-x, \Delta) \right), \qquad (49)$$

so that

$$F_f \approx \operatorname{sign}(v) \left(F_{\min} + \frac{F_{\max} - F_{\min}}{\Delta} \operatorname{mod}(\operatorname{sign}(v)x, \Delta) \right), \qquad (50)$$

where the constants $F_{\min}$ and $F_{\max}$ determine the minimum and maximum magnitudes of the friction force. The force F_f given by (50) is shown as a function of position in Figure 10(a) and as a function of velocity in Figure 10(b), where the position is prescribed to be $x(t) = A\sin(\omega t)$ and the velocity is $v(t) = A\omega\cos(\omega t)$, where $A = 1$ m and $\omega = 0.01$ rad/s.

3.5. Equilibria map

In this section we determine the equilibria of (40)-(41) arising from the friction force (47)-(49). The equilibria are found for each constant value $\bar{u}$ of the input $u(t)$. Due to the discontinuity of the friction force for $v = 0$, we use the approach of [38, 40] to analyze the equilibria.
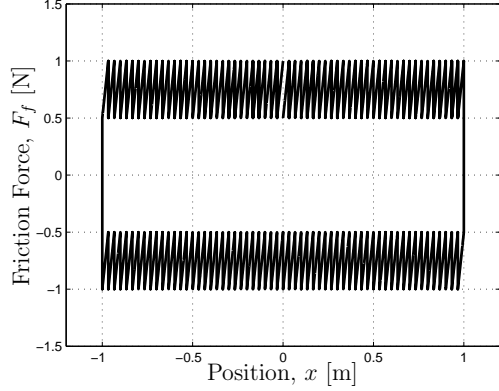
(a)
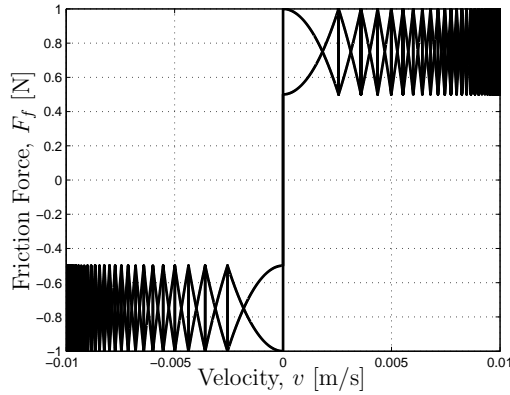
(b)

Figure 10: The approximation of the DRBM friction force (50) as a function of position (a) and velocity (b). The position is prescribed to be $x(t) = A\sin(\omega t)$ and velocity $v(t) = A\omega\cos(\omega t)$, where $A = 1$ m and $\omega = 0.01$ rad/s. The friction force parameters are $F_{\min} = 0.5$ N, $F_{\max} = 1$ N, and $\Delta = 0.033$ m.

We reformulate (40)-(41) as a differential inclusion (26) with $\boldsymbol{x} = \begin{bmatrix} x & v \end{bmatrix}^{\mathrm{T}}$ and vector fields $\boldsymbol{f}_+(\boldsymbol{x})$ and $\boldsymbol{f}_-(\boldsymbol{x})$ defined by (42) and (43), respectively. However, $F_{f+} = F_f^r$ and $F_{f-} = F_f^l$ are defined by (48) and (49), respectively. We set the input $u(t) = \bar{u}$ and determine the equilibria in the sets $\mathcal{V}_+$, $\mathcal{V}_-$, and Σ defined by (23), (24), and (25), respectively, with $g(\boldsymbol{x}) = v$. *The equilibria map $\mathcal{E}(\bar{u})$ is the set of all points $(\bar{u}, \bar{x}) \in \mathbb{R}^2$, such that $\bar{\boldsymbol{x}} = \begin{bmatrix} \bar{x} & \bar{v} \end{bmatrix}^{\mathrm{T}}$*

is an equilibrium of (26) corresponding to $u(t) = \bar{u}$.

To find equilibria in $\mathcal{V}_+$, we set $\boldsymbol{f}_+(\boldsymbol{x}) = 0$, which yields

$$\bar{x} = \frac{1}{K}(\bar{u} - F_{f+}), \tag{51}$$

$$\bar{v} = 0. \tag{52}$$

However, since $\mathcal{V}_+ = \{(x, v) : x \in \mathbb{R}, v > 0\}$ and $\bar{v} = 0$, the equilibrium $(\bar{x}, \bar{v})$ defined by (51) and (52) is not an element of $\mathcal{V}_+$, and thus there are no equilibria in $\mathcal{V}_+$. To find the equilibria in $\mathcal{V}_-$, we set $\boldsymbol{f}_-(\boldsymbol{x}) = 0$, which yields

$$\bar{x} = \frac{1}{K}(\bar{u} - F_{f-}), \tag{53}$$

$$\bar{v} = 0. \tag{54}$$

However, since $\mathcal{V}_- = \{(x, v) : x \in \mathbb{R}, v < 0\}$ and $\bar{v} = 0$, the equilibrium $(\bar{x}, \bar{v})$ defined by (53) and (54) is not an element of $\mathcal{V}_-$, and thus there are no equilibria in $\mathcal{V}_-$. Finally, to find the equilibria in Σ, we set

$$\boldsymbol{0} = \alpha \boldsymbol{f}_+(\boldsymbol{x}) + (1 - \alpha)\boldsymbol{f}_-(\boldsymbol{x}), \tag{55}$$

for all $\alpha \in [0, 1]$, which yields

$$\bar{x} \in \bar{\mathcal{X}}(\bar{u}) \triangleq \left\{ \frac{\bar{u} - (\alpha F_{f+} + (1 - \alpha)F_{f-})}{K} : \alpha \in [0, 1] \right\}, \tag{56}$$

$$\bar{v} = 0. \tag{57}$$

Since $\Sigma = \{(x, v) : x \in \mathbb{R}, v = 0\}$, it follows that all of the equilibria of (26) with $\boldsymbol{f}_+(\boldsymbol{x})$ and $\boldsymbol{f}_-(\boldsymbol{x})$ defined by (42) and (43), respectively, are elements of Σ. The equilibria map $\mathcal{E}(\bar{u})$ on the sliding manifold Σ is therefore given by

$$\mathcal{E}(\bar{u}) \triangleq \{(\bar{u}, \bar{x}) : \bar{u} \in \mathbb{R}, \bar{x} \in \bar{\mathcal{X}}(\bar{u})\}, \tag{58}$$

where $\bar{\mathcal{X}}(\bar{u})$ is defined by (56). The equilibria $(\bar{u}, \bar{x})$ in Σ are called *pseudo-equilibria* for $\alpha \in (0, 1)$ and *boundary equilibria* for $\alpha = 0$ or $\alpha = 1$ [40]. The set $\mathcal{E}(\bar{u})$ is shown in Figure 11. The shaded region represents the pseudo-equilibria, and the black lines represent the boundary equilibria. For

25

each constant input $\bar{u}$ there is an infinite number of corresponding pseudo-equilibria $\bar{x} \in \bar{\mathcal{X}}(\bar{u})$. The hysteresis map is also shown in Figure 11. Except for the vertical portions, the hysteresis map is a subset of the equilibria map. The vertical portions of the hysteresis map, which correspond to the slip phase, are not completely contained in the equilibria map since they occur at the points of bifurcations. For more details, see [41].
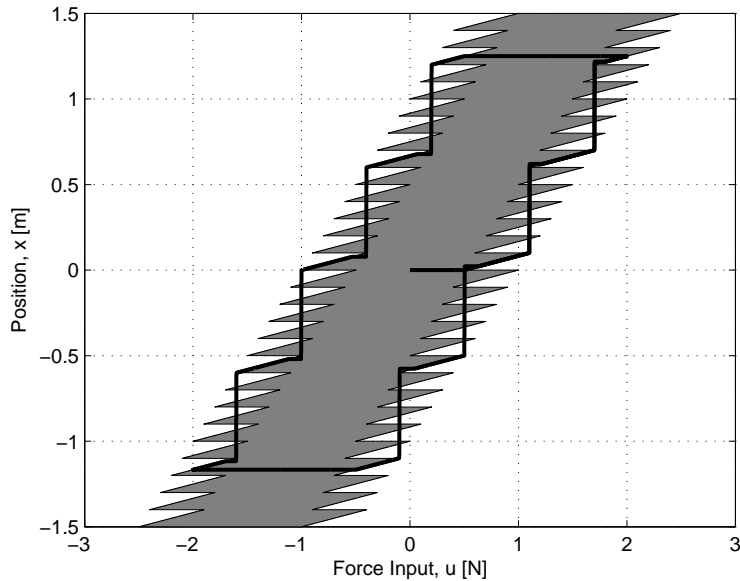

Figure 11: Equilibria and hysteresis maps of (40)-(41) with the friction force modeled by (47)-(49). The shaded area represents the pseudo-equilibria of the system. The boundary equilibria form the boundary of the shaded area. The hysteresis map, shown in black, is a subset of the equilibria map. The parameters used are $m = 1$ kg, $K = 1$ N/m, $\Delta = 0.1$ m, $F_{\min} = 0.5$ N, and $F_{\max} = 1$ N.

4. DRBM-based single-state models

In this section we introduce two simplified versions of the DRBM, namely, the friction-force-based model (FFBM) and the mean-pivot-angle-based model (MPABM). These versions eliminate the need for the Switch Model and yet capture the stick-slip behavior of the DRBM. The FFBM and MPABM are both single-state models [6, 35], as described below.

4.1. Single-state models

Single-state friction models such as the Dahl and LuGre model involve a state variable z that represents the internal friction mechanism. These models have the form

$$\dot{z} = v\left(1 - \alpha(v, z)\text{sign}(v)\frac{z}{z_{ss}(v)}\right), \tag{59}$$

$$F_f = \sigma_0 z + \sigma_1 \dot{z} + \sigma_2 v, \tag{60}$$

where σ_0, σ_1, σ_2 are positive constants, z is the internal friction state, $z_{ss}(v)$ determines the shape of the steady-state z curve, and F_f is the friction force. The function $\alpha(v, z)$ determines the presence and type of elastoplastic presliding displacement [35, 42]. For simplicity, we set $\alpha(v, z) = 1$ and rewrite (59)-(60) as

$$\dot{z} = v - \frac{|v|}{z_{ss}(v)}z, \tag{61}$$

$$F_f = \sigma_0 z + \sigma_1 \dot{z} + \sigma_2 v. \tag{62}$$

Setting $z_{ss}(v)$ to be

$$z_{ss}(v) = \frac{1}{\sigma_0}\left(F_c + (F_s - F_c)e^{-(v/v_s)^2}\right), \tag{63}$$

where F_c, F_s, and v_s are constants, yields the LuGre model [14, 15], which exhibits stick-slip, hysteresis, and the Stribeck effect.

In steady-state motion, $\dot{z} = 0$, and thus $z = \text{sign}(v)z_{ss}(v)$. Furthermore, if $\sigma_1 = \sigma_2 = 0$, then

$$F_f = \sigma_0 z = \text{sign}(v)\sigma_0 z_{ss}(v). \tag{64}$$

4.2. Friction-force-based model (FFBM)

The friction-force-based model (FFBM) is formulated by using the approximation (50) of the DRBM friction force to define z_{ss}. Equating (50) with (64) yields

$$z_{ss}(v, x) = \frac{1}{\sigma_0}\left(F_{\min} + \frac{F_{\max} - F_{\min}}{\Delta}\text{mod}\left(\text{sign}(v)x, \Delta\right)\right), \tag{65}$$

and thus (61)-(62) become

$$\dot{z} = v - \sigma_0 \frac{|v|}{F_{\min} + \frac{F_{\max} - F_{\min}}{\Delta} \operatorname{mod}(\operatorname{sign}(v)x, \Delta)} z, \tag{66}$$

$$F_f = \sigma_0 z. \tag{67}$$

In this case, z has the units of force and can be viewed as the contribution of one bristle to the total friction force, while the total number of bristles contributes to the friction force through the parameter σ_0. Note that, unlike $z_{ss}(v)$ in (61), the term $z_{ss}(v, x)$ in (65) depends on both position and velocity.

We now consider the system shown in Figure 8 and described by (40)-(41) with the external force $u(t)$ and the friction force modeled by (66)-(67). The complete system of equations is

$$\dot{x} = v, \tag{68}$$

$$\dot{v} = \frac{1}{m}(-Kx + u - F_f), \tag{69}$$

$$\dot{z} = v - \sigma_0 \frac{|v|}{F_{\min} + \frac{F_{\max} - F_{\min}}{\Delta} \operatorname{mod}(\operatorname{sign}(v)x, \Delta)} z, \tag{70}$$

$$F_f = \sigma_0 z. \tag{71}$$

For each constant force input $u(t) = \bar{u}$ the equilibria of (68)-(71) are

$$\bar{x} = \frac{1}{K}(\bar{u} - \sigma_0 \bar{z}), \tag{72}$$

$$\bar{v} = 0, \tag{73}$$

$$\bar{z} = \operatorname{sign}(0)\frac{1}{\sigma_0}\left(F_{\min} + \frac{F_{\max} - F_{\min}}{\Delta} \operatorname{mod}(\operatorname{sign}(0)\bar{x}, \Delta)\right). \tag{74}$$

By viewing $\operatorname{sign}(0)$ as the interval $[-1, 1]$ we rewrite (74) as

$$\bar{z} \in \bar{\mathcal{Z}} \triangleq \left\{(2\alpha - 1)\frac{1}{\sigma_0}\left(F_{\min} + \frac{F_{\max} - F_{\min}}{\Delta} \operatorname{mod}((2\alpha - 1)\bar{x}, \Delta)\right) : \alpha \in [0, 1]\right\}. \tag{75}$$

Note that (75) is equivalent to

$$\bar{z} \in \bar{\mathcal{Z}} \triangleq \left\{ \frac{1}{\sigma_0} \left(\alpha F_f^r + (1-\alpha) F_f^l \right) : \alpha \in [0,1] \right\}, \tag{76}$$

where F_f^r and F_f^l are defined by (48) and (49), respectively. Substituting (76) into (72) gives the equilibria map of (68)-(71)

$$\mathcal{E}(\bar{u}) = \{ (\bar{u}, \bar{x}) : \bar{u} \in \mathbb{R}, \ \bar{x} \in \bar{\mathcal{X}}(\bar{u}) \}, \tag{77}$$

where

$$\bar{\mathcal{X}}(\bar{u}) = \left\{ \frac{\bar{u} - (\alpha F_f^r + (1-\alpha) F_f^l)}{K} : \alpha \in [0,1] \right\}, \tag{78}$$

which is identical to the equilibria set (58) for the DRBM on the sliding manifold.

The equilibria set and the hysteresis map of (68)-(71) are shown in Figure 12. The system is hysteretic and exhibits exact stick-slip, where the exact stick-slip is demonstrated by the staircase-shaped hysteresis map. The parameters used are $m = 1$ kg, $K = 1$ N/m, $F_{\min} = 1$ N, $F_{\max} = 1.5$ N, $\Delta = 0.05$ m, $u(t) = 2\sin(\omega t)$ N, $\omega = 0.01$ rad/s, $\sigma_0 = 10^5$. The hysteresis map is a subset of the equilibria set, except for the vertical portions, which correspond to the slip phases and occur at bifurcation points [41].

4.3. Mean-pivot-angle-based model (MPABM)

We develop the mean-pivot-angle-based model (MPABM) by assuming that the sum θ_s of the pivot angles θ_i of all of the bristles contributing to the friction force can be approximated by its exponentially weighted moving average (EWMA) $\bar{\theta}$ [43, 44]. The goal is to express $\bar{\theta}$ as a function of v, so that setting $z_{ss}(v) = \bar{\theta}(v)$ yields a single-state friction model.

To find $\bar{\theta}$ at each discrete time step t_j, we use

$$\bar{\theta}(t_j) = \beta \theta_s(t_j) + (1-\beta)\bar{\theta}(t_j - 1), \tag{79}$$

where $\beta \in [0,1]$ is a constant, $\bar{\theta}(0) = \theta_s(0)$, and the weighting for the data point $\theta_s(t_j - i)$ is $\beta(1-\beta)^{i-1}$, that is, the weighting for prior data points decreases exponentially [43, 44].
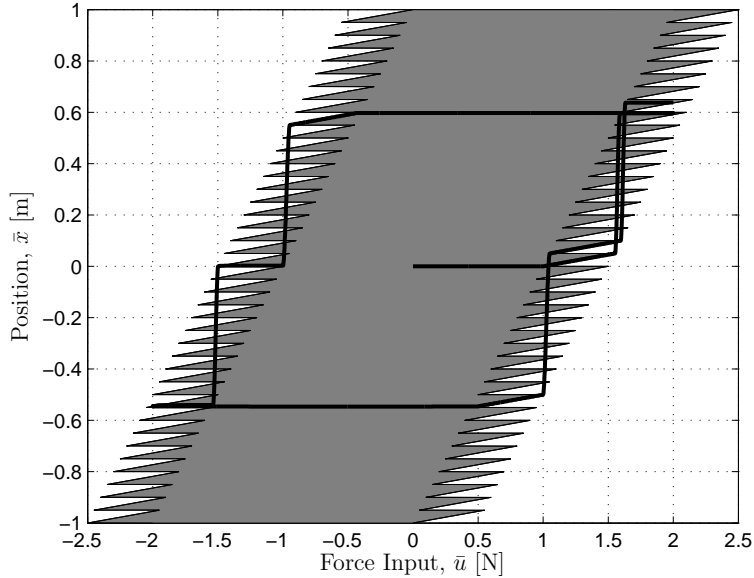
Figure 12: Equilibria map and hysteresis map of (68)-(71) with force input $u(t) = 2\sin(\omega t)$ with $m = 1$ kg, $K = 1$ N/m, $F_{\min} = 1$ N, $F_{\max} = 1.5$ N, $\Delta = 0.05$ m, $\omega = 0.01$ rad/s, and $\sigma_0 = 10^5$.

Since $\bar{\theta}$ can be interpreted as a pivot angle of a single bristle that is contributing to the friction force, the vectors Θ_r and Θ_l used to calculate F_f in (13) and (15) are replaced by $\bar{\theta}$, and (13) and (15) are replaced by

$$F_f = \frac{\kappa\bar{\theta}(\cos\bar{\theta})^2}{h} \approx \frac{\kappa}{h}\bar{\theta}, \tag{80}$$

for small angles $\bar{\theta}$.

We use (79) to find $\bar{\theta}$ for the differential inclusion (26) with $\boldsymbol{f}_+$ and $\boldsymbol{f}_-$ defined by (38)-(39), respectively. The sum θ_s of all of the bristle pivot angles is shown in Figure 13(a). The model parameters are $m = 1$ kg, $K = 1$ N/m, $v_p = 0.002$ m/s, $d = 0.5$ N, $\kappa = 0.1$ N-m/rad, $h = 0.0995$ m, $l_b = 0.1$ m, $d_0 = 0.01$ m, $\Delta = 0.005$ m, and $\eta = 10^{-8}$. Figure 13(b) shows $\bar{\theta}(t_j)$ found from (79) with $\beta = 0.05$, as a function of time and Figure 13(c) as a function of velocity. The two traces in Figure 13(c) represent $\bar{\theta}(t_j)$ corresponding to increasing and decreasing velocity.

As shown by the dashed line in Figure 14, the dependence of $\bar{\theta}$ on velocity

(a)   (b)   (c)
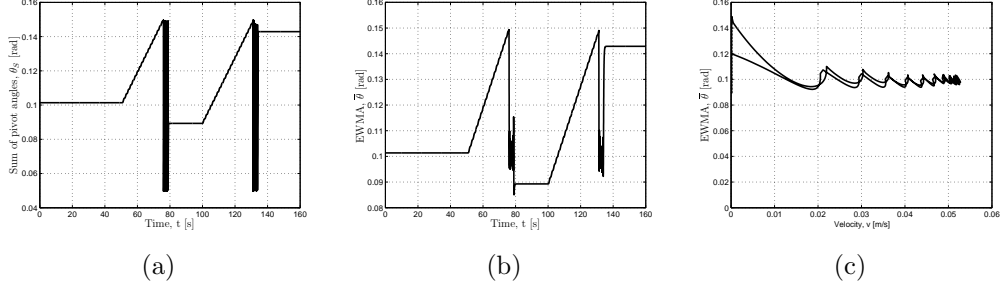
Figure 13: Sum of the pivot angles θ_s of all of the bristles contributing to the friction force (a), the EWMA of θ_s as a function of time (b) and as a function of velocity (c). The pivot angle data are obtained from the simulation of (38) and (39) with parameters $m = 1$ kg, $K = 1$ N/m, $v_p = 0.002$ m/s, $d = 0.5$ N, $\kappa = 0.1$ N-m/rad, $h = 0.0995$ m, $l_b = 0.1$ m, $d_0 = 0.01$ m, $\Delta = 0.005$ m, and $\eta = 10^{-8}$. The EWMA is found from (79) with $\beta = 0.05$. The two traces in (c) represent $\overline{\theta}(t_j)$ for increasing and decreasing values of velocity.

shown in Figure 13(c) can be approximated by

$$\overline{\theta} \approx \hat{\overline{\theta}}(v) \triangleq \text{sign}(v) \left(\hat{\theta}_{\min} + (\hat{\theta}_{\max} - \hat{\theta}_{\min})e^{-(v/\hat{v}_s)^2} \right), \tag{81}$$

where $\hat{\theta}_{\min} = 0.1$ rad, $\hat{\theta}_{\max} = 0.133$ rad, and $\hat{v}_s = 0.01$ m/s. The parameters $\hat{\theta}_{\max}$ and $\hat{\theta}_{\min}$ are determined by the values of $\overline{\theta}$ for $v = 0$ m/s and $v \to \infty$, respectively. In addition, the parameter $\hat{v}_s$ reflects the decay rate of $\overline{\theta}$, which is determined by the choice of β. Combining (80) and (81) yields the mean friction force expression

$$\overline{F_f} = \frac{\kappa}{h}\text{sign}(v) \left(\hat{\theta}_{\min} + (\hat{\theta}_{\max} - \hat{\theta}_{\min})e^{-(v/\hat{v}_s)^2} \right), \tag{82}$$

so that

$$z_{ss}(v) = \frac{1}{\sigma} \left(\hat{\theta}_{\min} + (\hat{\theta}_{\max} - \hat{\theta}_{\min})e^{-(v/\hat{v}_s)^2} \right), \tag{83}$$

and the single-state friction model equations are

$$\dot{z} = v - \sigma \frac{|v|}{\hat{\theta}_{\min} + (\hat{\theta}_{\max} - \hat{\theta}_{\min})e^{-(v/\hat{v}_s)^2}} z, \tag{84}$$

$$F_f = \sigma_0 z, \tag{85}$$

31

where $\sigma_0 = \frac{\kappa}{h}\sigma$. The single-state friction model (84)-(85) is the LuGre model (61)-(63) with $\sigma = \sigma_0$, $\sigma_1 = 0$, $\sigma_2 = 0$. Note that, the Stribeck effect of the MPABM is an artifact of the approximation of θ_s by its EWMA $\bar{\theta}$ and is not a property inherited from the DRBM.
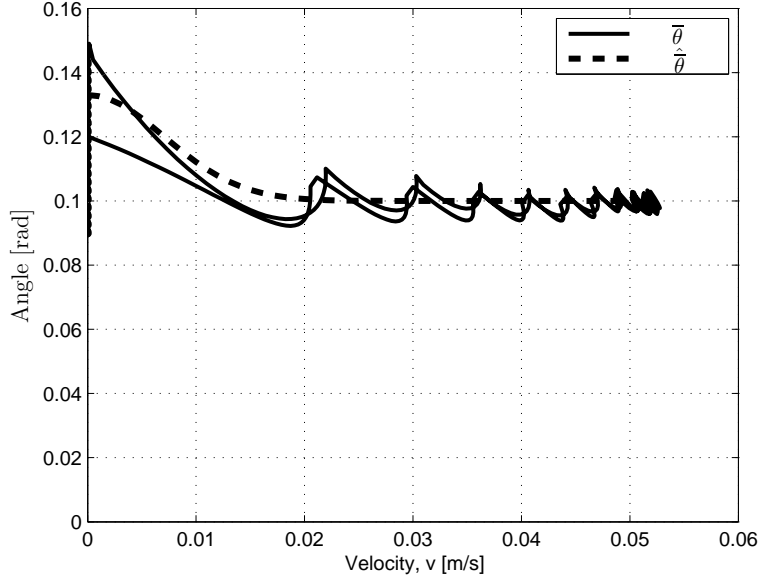

Figure 14: The EWMA $\bar{\theta}$ (solid) of the sum of all pivot angles and its approximation $\hat{\bar{\theta}}$ (dashed). The EWMA is found from (79) with $\beta = 0.05$ and can be approximated by $\hat{\bar{\theta}} = \text{sign}(v)\left(\hat{\theta}_{\min} + (\hat{\theta}_{\max} - \hat{\theta}_{\min})e^{-(v/\hat{v}_s)^2}\right)$, where $\hat{\theta}_{\min} = 0.1$ rad, $\hat{\theta}_{\max} = 0.133$ rad, and $\hat{v}_s = 0.01$ m/s.

We use (84) and (85) to represent the friction force of the system shown in Figure 8 and described by (40)-(41). The complete description is

$$\dot{x} = v, \tag{86}$$

$$\dot{v} = \frac{1}{m}(-Kx + u - F_f), \tag{87}$$

$$\dot{z} = v - \sigma\frac{|v|}{\hat{\theta}_{\min} + (\hat{\theta}_{\max} - \hat{\theta}_{\min})e^{-(v/\hat{v}_s)^2}}z, \tag{88}$$

$$F_f = \sigma_0 z, \tag{89}$$

and, for each constant value of the input $u(t) = \bar{u}$, the equilibria of this

system are

$$\bar{x} = \frac{1}{K}(\bar{u} - \sigma_0 \bar{z}), \tag{90}$$

$$\bar{v} = 0, \tag{91}$$

$$\bar{z} = \text{sign}(0)\frac{1}{\sigma}\hat{\theta}_{\max}. \tag{92}$$

By viewing $\text{sign}(0)$ as the interval $[-1, 1]$, the equilibria map of (86)-(89) is the set

$$\mathcal{E}(\bar{u}) = \{(\bar{u}, \bar{x}) : \bar{u} \in \mathbb{R}, \ \bar{x} \in \bar{\mathcal{X}}(\bar{u})\}, \tag{93}$$

where

$$\bar{\mathcal{X}}(\bar{u}) = \left\{ \frac{1}{K}\left(\bar{u} - \frac{\kappa}{h}(2\alpha - 1)\hat{\theta}_{\max}\right) : \alpha \in [0, 1]\right\}. \tag{94}$$

The equilibria set (93) and the hysteresis map of the system (86)-(89) are shown in Figure 15 with parameters $u(t) = 2\sin(\omega t)$, $m = 1$ kg, $K = 2$ N/m, $\theta_{\min} = 0.5$ rad, $\theta_{\max} = 0.75$ rad, $\omega = 0.01$ rad/s, $\sigma_0 = 10^5$ N/rad, $\sigma = 10^5$, and $v_s = 0.001$ m/s. The equilibria set is the region shaded gray. For each constant force input $\bar{u}$ there is an infinite number of corresponding equilibria points. Thus, the system is hysteretic and the hysteresis map is a subset of the equilibria map. Furthermore, the staircase-shaped hysteresis map indicates exact stick-slip motion.

5. Conclusions

In this paper we developed an asperity-based friction model. The friction model is based on the frictionless and lossless interaction of a body with a row of rigid bristles that represent the roughness of the contacting surfaces. Each bristle in the rotating bristle model is attached to the ground through a torsional spring and a dashpot. As the body moves, the bristles pivot and counteract its motion, and energy is used to compress the spring at the base of each bristle. As the body passes over each bristle, it is suddenly released, and the energy stored in its spring is dissipated by a dashpot. The resulting energy loss occurs regardless of how slowly the mass moves. Consequently, the bristle model is hysteretic.
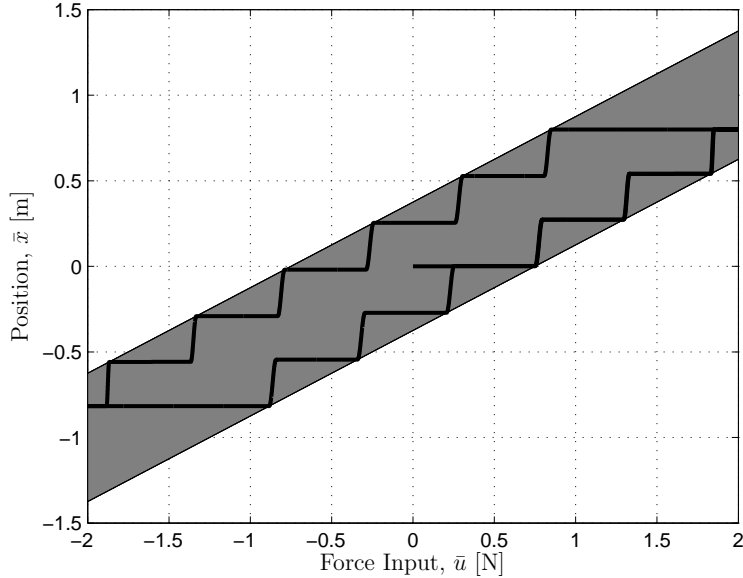
Figure 15: Equilibria map and hysteresis map of (86)-(89) with force input $u(t) = 2\sin(\omega t)$ with $m = 1$ kg, $K = 2$ N/m, $\theta_l = 0.5$ rad, $\theta_h = 0.75$ rad, $\omega = 0.01$ rad/s, $\sigma_0 = 10^5$ N/rad, $\sigma = 10^5$, and $v_s = 0.001$ m/s. The equilibria map forms a continuum shown in gray shade and the hysteresis map is shown in thick black.

The rotating bristle model exhibits quasi-stick-slip, similar to exact stick-slip but where the stick phase is replaced by reverse motion. Thus, we introduce the discontinuous rotating bristle model (DRBM), which exhibits exact stick-slip and hysteresis and is identical to the rotating bristle model except during direction reversals.

We then simplify the DRBM to obtain single-state friction models that are continuous and have the same stick-slip properties as the DRBM. For the FFBM single-state model, the internal friction state represents the contribution of each bristle to the friction force. For the MPABM, the internal friction state is given by the exponentially weighted moving average of the sum of the pivot angles of all of the bristles contributing to the friction force. The FFBM and MPABM models exhibit exact stick-slip and hysteresis and are closely related to the LuGre model. Thus, we show that the frictionless interaction of the bristles and a body results in the friction force that has the properties of experimentally based friction models such as LuGre.

34

References

[1] B. Armstrong-Hélouvry, Control of Machines with Friction, Kluwer, Boston, MA, 1991.

[2] B. Armstrong-Hélouvry, P. Dupont, C. C. de Wit, A survey of models, analysis tools and compensation methods for the control of machines with friction, Automatica 30 (1994) 1083–1138.

[3] I. D. Mayergoyz, Mathematical Models of Hysteresis, Elsevier, 2003.

[4] A. Visintin, Differential Models of Hysteresis, Springer-Verlag, New York, 1994.

[5] M. A. Krasnosel'skii, A. V. Pokrovskii, Systems with Hysteresis, Springer-Verlag, New York, 1980.

[6] J. J. Choi, S. I. Han, J. S. Kim, Development of a novel dynamic friction model and precise tracking control using adaptive back-stepping sliding mode controller, Mechatronics 16 (2006) 97–104.

[7] K. K. Leang, Q. Zou, S. Devasia, Feedforward control of piezoactuators in atomic force microscope systems, IEEE Contr. Sys. Mag. 29 (2009) 70–82.

[8] T. Sakamoto, Normal displacement and dynamic friction characteristics in a stick-slip process, Tribology International 20 (1987) 25–31.

[9] D. M. Tolstoi, Significance of the normal degree of freedom and natural normal vibrations in contact friction, Wear 10 (1967) 199–213.

[10] J. A. C. Martins, J. T. Oden, F. M. F. Simoes, Recent advances in engineering science: A study of static and kinetic friction, Int. J. Eng. Sci. 28 (1990) 29–92.

[11] A. K. Padthe, B. Drincic, J. Oh, D. D. Rizos, S. D. Fassois, D. S. Bernstein, Duhem modeling of friction-induced hysteresis: Experimental determination of gearbox stiction, IEEE Contr. Sys. Mag. 28 (2008) 90–107.

[12] A. K. Padthe, N. A. Chaturvedi, D. S. Bernstein, S. P. Bhat, A. M. Waas, Feedback stabilization of snap-through buckling in a preloaded two-bar linkage with hysteresis, Int. J. Non-Linear Mech. 43 (2008) 277–291.

[13] H. Olsson, K. J. Åström, C. Canudas de Wit, M. Gafvert, P. Lischinsky, Friction models and friction compensation, European Journal of Control 4 (1998) 176–195.

[14] K. J. Astrom, C. Canudas-De-Wit, Revisiting the LuGre friction model, IEEE Contr. Sys. Mag. 28 (2008) 101–114.

[15] F. Avanzini, S. Serafin, D. Rocchesso, Modeling interaction between rubbed dry surfaces using an elasto-plastic friction model, in: Proc. 5th Int. Conference on Digital Audio Effects, Hamburg, Germany, pp. 111–116.

[16] C. Canudas de Wit, H. Olsson, K. J. Åström, P. Lischinsky, A new model for control of systems with friction, IEEE Trans. Autom. Contr. 40 (1995) 419–425.

[17] N. Barabanov, R. Ortega, Necessary and sufficient conditions for passivity of the lugre friction model, IEEE Trans. Autom. Contr. 45 (2000) 675–686.

[18] C. Makkar, W. E. Dixon, W. G. Sawyer, G. Hu, A new continuously differentiable friction model for control systems design, in: IEEE/ASME Int. Conf on Adv. Intell. Mechatronics, Monterey, CA, pp. 600–605.

[19] S. H. Park, J. S. Kim, J. J. Choi, H.-O. Yamazaki, Modeling and control of adhesion force in railway rolling stocks: Adaptive sliding mode control for the desired wheel slip, IEEE Contr. Sys. Mag. 28 (2008) 44–58.

[20] C. Makkar, G. Hu, W. G. Sawyer, W. E. Dixon, Lyapunov-based tracking control in presence of uncertain nonlinear parameterizable friction, IEEE Trans. Autom. Contr. 52 (2007) 1988–1994.

[21] J. Swevers, F. Al-Bender, C. G. Ganseman, T. Prajogo, An integrated friction model structure with improved presliding behavior for accurate friction compensation, IEEE Trans. Autom. Contr. 45 (2000) 675–686.

[22] Y. Guo, Z. Qu, Y. Braiman, Z. Zhang, J. Barhen, Nanotribology and nanoscale friction: Smooth sliding through feedback control, IEEE Contr. Sys. Mag. 28 (2008) 92–100.

[23] B. S. R. Armstrong, Q. Chen, The z-properties chart: Visualizing the presliding behavior of state-variable friction models, IEEE Contr. Sys. Mag. 28 (2008) 79–89.

[24] D. A. Haessig, B. Friedland, On the modeling and simulation of friction, ASME J. Dyn. Sys. Meas. Contr. 113 (1991) 354–361.

[25] N. E. Dowling, Mechanical Behavior of Materials: Engineering Methods for Deformation, Fracture, and Fatigue, Prentice Hall, Englewood Cliffs, NJ, 1993.

[26] F. Al-Bender, J. Swevers, Characterization of friction force dynamics: Behavior and modeling on micro and macro scales, IEEE Contr. Sys. Mag. 28 (2008) 82–91.

[27] D. S. Bernstein, Ivory ghost, IEEE Control Systems Magazine 27 (2007) 16–17.

[28] D. M. Rowson, An analysis of stick-slip motion, Wear 31 (1975) 213–218.

[29] H. Olsson, K. J. Åström, Friction generated limit cycles, IEEE Trans. Contr. Sys. Tech. 9 (2001) 629–636.

[30] R. I. Leine, D. H. V. Campen, A. De Kraker, L. Van Den Steen, Stick-slip vibrations induced by alternate friction models, Nonlinear Dynamics 16 (1998) 41–45.

[31] N. B. Do, A. A. Ferri, O. A. Bauchau, Efficient simulation of a dynamic system with LuGre friction, Journal of Computational and Nonlinear Dynamics 2 (2007) 281–289.

[32] L. C. Bo, D. Pavelescu, The friction-speed relation and its influence on the critical velocity of stick-slip motion, Wear 82 (1982) 277–289.

[33] C. J. Radcliffe, S. C. Southward, A property of stick-slip friction models which promotes limit cycle generation, in: Proc. Amer. Contr. Conf., volume 2, pp. 1198–1203.

[34] A. F. D'Souza, A. H. Dweib, Self-excited vibrations induced by dry friction, part 2: Stability and limit-cycle analysis, Journal of Sound and Vibration 137 (1990) 177–190.

[35] P. Dupont, V. Hayward, B. Armstrong, F. Altpeter, Single state elasto-plastic friction models, IEEE Trans. Autom. Contr. 47 (2002) 787–792.

[36] B. Drinčić, D. S. Bernstein, A sudden-release bristle model that exhibits hysteresis and stick-slip friction, in: Proc. Amer. Contr. Conf., San Francisco, CA, pp. 2456 – 2461.

[37] R. I. Leine, H. Nijmeijer, Dynamics and bifurcations of non-smooth mechanical systems, Springer, Berlin, 2004.

[38] A. F. Filippov, Differential Equations with Discontinuous Righthand Sides, Kluwer Academic Publishers, Dordrecht, The Netherlands, 1988.

[39] J. Oh, D. S. Bernstein, Semilinear Duhem model for rate-independent and rate-dependent hysteresis, IEEE Trans. Autom. Contr. 50 (2005) 631–645.

[40] M. di Bernardo, C. J. Budd, A. R. Campneys, P. Kowalczyk, Piecewise-smooth Dynamical Systems, Springer-Verlag, London, UK, 2008.

[41] J. Oh, B. Drincic, D. S. Bernstein, Nonlinear feedback models of hysteresis, IEEE Control Systems Magazine 29 (2009) 100–119.

[42] P. Dupont, B. Armstrong, V. Hayward, Elasto-plastic friction model: Contact compliance and stiction, in: Proc. Amer. Contr. Conf., Chicago, IL, pp. 1072–1077.

[43] G. E. P. Box, G. M. Jenkins, G. C. Reinsel, Time Series Analysis: Forecasting and Control, Wiley, Hoboken, New Jersey, 2008.

[44] C. C. Holt, Forecasting seasonals and trends by exponentially weighted moving averages, Int. J. Forecasting 20 (2004) 5–10.